A flow rate soft sensor for pumps with complex characteristics

Sebastian Leonow * **Qi Zhang** ** **Martin Mönnigmann** ***

* (e-mail: sebastian.leonow@ruhr-uni-bochum.de)
** (e-mail: Qi.Zhang-x92@ruhr-uni-bochum.de)
*** (e-mail: martin.moennigmann@ruhr-uni-bochum.de)
Automatic Control and System Theory, Department of Mechanical Engineering, Ruhr University Bochum, Universitätstrasse 150, 44801 Bochum, Germany.

Abstract: Flow rate soft sensors have become an important alternative for costly hardware flow meters, as they can estimate the flow rate with sufficient precision from easily measurable variables by using models and state estimation algorithms. This paper addresses the fundamental challenge that arises from ambiguous estimation problems, where the measured variable corresponds to two or more possible flow rate values. We develop and implement a decision algorithm that yields correct results in an industrial setup with substantial measurement noise. The results demonstrate a reliable flow rate estimation, providing a viable solution for real-time flow monitoring in centrifugal pumps with complex characteristics.

Keywords: Smart Sensors and Actuators, Kalman filtering, Centrifugal Pump, Flow Rate Estimation

1. INTRODUCTION

Nearly 20% of global electricity is consumed by pumping systems (Shankar et al., 2016). Of all pump types, centrifugal pumps are most widely used in many industries, including petroleum, chemicals, energy, and water treatment (Lin et al., 2022; Sedghi et al., 2020). Because of their wide range of application, improving the efficiency of centrifugal pumps holds a significant energy savings potential (Ahonen et al., 2010; Leonow et al., 2024). To ensure that centrifugal pumps operate at their Best Efficient Point (BEP), obtaining real-time flow rate data is crucial. While traditional hardware flow sensors, such as turbine or electromagnetic flow meters, provide accurate measurements, their high cost, complex installation, and maintenance requirements limit their industrial use. As a consequence, flow rate soft sensors have gained increased interest and research in recent years (Sedghi et al., 2020; Leonow et al., 2024).

The concept of soft sensors involves using easily measurable variables to estimate target variables through modeling and state estimation algorithms (Becker and Krause, 2010). Several flow rate soft sensor architectures have been successfully used in simulations and experimental studies. For example, Lima et al. (2022) contribute to flow estimation of centrifugal pumps with an artificial neural network based soft sensor, with results showing a maximum error of 10% compared to an electromagnetic flux sensor. Wu et al. (2023) address varying hydraulic process parameters with a Genetic Algorithm, Back-Propagation Neural Network model, achieving an average flow rate estimation error of less than 2%. Changklom and Stoianov (2019) proposed a distributed pressure measurement with three sensors at different locations within the centrifugal pump and demonstrated a precise flow rate estimation based on the pressure information. Applying an array of ultrasonic level sensors in combination with a neural network, fuzzy logic, and support vector regression algorithms, showed high reliability and accuracy of flow rate estimation in oil and gas and geothermal installations (Chhantyal et al., 2017).

Compared to the significant progress in simulation and experimental studies, the industrial application of flow rate soft sensors clearly falls behind (Leonow et al., 2024), which can partly be accounted to the high noise levels in industrial process data Ren et al. (2021). In addition to challenges due to noise, around 20% of centrifugal pumps show non-invertible (non-monotone) characteristics. This implies that several distinct flow rates result in the same pump head or shaft power. This non-uniqueness poses a fundamental problem for soft sensors and essentially renders current estimation methods impractical (Shankar et al., 2016; Leonow and Mönnigmann, 2016).

While sensor fusion is one way to address this issue, e.g. by combining pressure and electrical power measurements (KSB-AG, 2005), this approach again requires the costly installation of additional sensors. As an alternative, Leonow and Mönnigmann (2016) proposed a dynamic excitation of the hydraulic process to acquire sufficient information for inferring the correct flow rate estimate with only a single sensor measuring electrical power, which proved viable in simulations. However, the approach proposed in Leonow and Mönnigmann (2016) has so far not been validated in a practical application. Moreover, it requires a dominant fluid inertia, which limits the application of the algorithm. Building on this prior work, this paper introduces a practical approach for the decision between two possible flow rate estimates. We conduct real-time testing under high-noise conditions on a centrifugal pump with non-invertible characteristic to validate the algorithm's effectiveness.

2. NOTATION AND PRELIMINARIES

We assume a fixed mechanical coupling between motor and pump and introduce f as the rotational frequency of motor and pump and i as the electrical current drawn by the motor. The hydraulic power that the pump provides is P and we assume $i \propto P$. The flow rate through the pump is q. The hydraulic plant in which the pump is integrated dissipates hydraulic power P_{P}. We use subscripts meas for measured values, mod for simulated (model) values, norm for a dataset or function that is scaled onto an interval $[0,1]$, and min, max for minimal and maximal values in a dataset. A hat denotes estimated values and a superscript * denotes values that result from a decision process.

In steady state, i.e. $\mathrm{d}q/\mathrm{d}t = \mathrm{d}i/\mathrm{d}t = \mathrm{d}P_{\mathrm{P}}/\mathrm{d}t = 0$, the hydraulic powers provided by the pump and consumed by the plant coincide, i.e. $P = P_{\mathrm{P}}$. Following the hydraulic affinity laws we assume $q \propto f$, $i \propto f$, $i \propto q^3$, and $P_{\mathrm{P}} \propto q^3$ hold.

A frequency step is given by Δf, and the actual frequency after applying the frequency step is $f = \overline{f} - \Delta f$ with $\overline{f}$ being the steady-state or initial frequency.

Generally, pump characteristic curves can be categorized into three types: invertible, simple non-invertible, and repeatedly non-invertible, as illustrated in Fig. 1. An invertible curve indicates a one-to-one relationship between the flow rate and the measured variable (i.e. pump head, shaft power, or electrical current), allowing in a unique estimation of the flow rate based on the single measured variable. In contrast, a typical non-invertible characteristic implies that e.g. a measured electrical power may correspond to two different flow rates. The third type, repeatedly non-invertible characteristic, allows more than two flow rates to map to the same measured variable. The shape of the characteristics can change with the rotational speed and an ambiguous characteristic is more likely for higher speeds than for lower speeds (see Fig. 2).

We focus on the significantly more common, simple non-invertible characteristic in this paper.

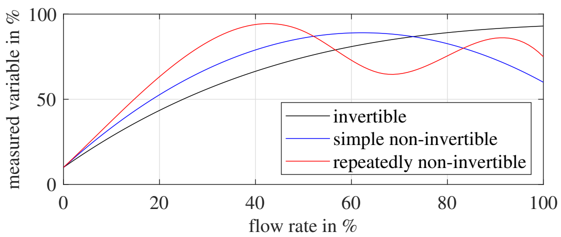

Fig. 1. Sketches of characteristics of centrifugal pumps.

3. FLOW RATE ESTIMATION METHOD

We choose the electrical current i and the frequency f as measurements to drive the flow rate estimation. An Unscented Kalman Filter (UKF) serves as baseline estimator. The filter is augmented by a decision algorithm (see Sec. 3.3) that identifies the correct estimate in the ambiguous sections of the $q \to i$ characteristic. We will outline the core estimation model as part of the UKF in the following section, followed by the UKF implementation, for ease of result interpretation. The primary contribution of this paper is the decision algorithm, which is essentially independent of the specific estimator or plant model.

3.1 System Model

We choose a data-based modeling approach to capture the motor-pump system in an input-output sense. The model architecture is similar to the Boundary Curve method Leonow and Mönnigmann (2013). While the original method assumed that the shape of the $q \to i$ characteristic is unique for all frequencies, we incorporate the frequency and map $f, q \to i$. While this approach is more elaborate in terms of data acquisition, the resulting improvement in soft sensor precision is superior. Fig. 2 depicts measured $q \to i$ curves for four different frequencies. The shape of the $q \to i$ curves obviously depends on the frequency here, ranging from invertible at lower frequencies to simple non-invertible towards the design frequency $f = 50\mathrm{Hz}$.

More specifically, for a set of frequencies $f \in (f_{\min}, f_{\max})$, the minimum and maximum boundaries of q and i are measured, where the boundaries are defined by the lowest and highest admissible flow rates $\min(q)$ and $\max(q)$, respectively. The measurement results in four boundary curves $q_{\min}(f) := f \to \min(q)$, $q_{\max}(f) := f \to \max(q)$, $i_{\min}(f) := f \to i(\min(q))$, and $i_{\max}(f) := f \to i(\max(q))$. We approximate the $f \to q$ maps with linear functions

$$q_{\min}(f) = c_{q,\min} \cdot f \ , \quad q_{\max}(f) = c_{q,\max} \cdot f \tag{1}$$

and the $f \to i$ maps with a cubic function

$$i_{\min}(f) = \sum_{k=0}^{3} c_{i,\min,k} \cdot f^k \ , \quad i_{\max}(f) = \sum_{k=0}^{3} c_{i,\max,k} \cdot f^k \ , \tag{2}$$

in accordance with the hydraulic affinity laws. Parameters c_x result from least squares optimizations based on the measured data. With (1),

$$q_{\mathrm{norm}} = \frac{q - q_{\min}(f)}{q_{\max}(f) - q_{\min}(f)} \tag{3}$$

normalizes a given flow rate q to the range $[0,1]$. With (2),

$$i = i_{\mathrm{norm}} \cdot (i_{\max}(f) - i_{\min}(f)) + i_{\min}(f) \tag{4}$$

scales a normalized current $i_{\mathrm{norm}} \in (0,1)$ back to its physical range. The map between q_{norm} and i_{norm} is captured by a two-dimensional lookup-table

$$f, q_{\mathrm{norm}} \to i_{\mathrm{norm}} \ . \tag{5}$$

The complete, nonlinear-static model results from the combination of (3) - (5). We stress here that also for non-invertible characteristics, the model $f, q \to i$ is still one-to-one. Fig. 2 depicts the model structure and the $f, q_{\mathrm{norm}} \to i_{\mathrm{norm}}$ curves for the sample pump used for evaluation.

The original Boundary Curve method (Leonow and Mönnigmann (2013)) assumes a linear dynamic model part to capture lag effects, e.g. from pump inertia. With a series of step responses, measured with $q = 0$, thus excluding any flow rate related effects, a n-th order state space model

$$
x_i(k+1) = \underbrace{\begin{pmatrix} 0 & 1 & 0 & \dots & 0 \\ 0 & 0 & 1 & \dots & 0 \\ \vdots & \vdots & \vdots & \ddots & \vdots \\ 0 & 0 & 0 & \dots & 1 \\ 0 & 0 & 0 & \dots & 0 \end{pmatrix}}_{A} \cdot x_i(k) + \underbrace{\begin{pmatrix} 0 \\ 0 \\ 0 \\ \vdots \\ 1 \end{pmatrix}}_{b} \cdot i(f,q)
$$

$$
i_{\mathrm{mod}}(k) = \underbrace{\begin{pmatrix} c_{i,1} & c_{i,2} & \dots & c_{i,n} \end{pmatrix}}_{c} \cdot x_i(k) \tag{6}
$$

is identified, where the coefficients $c_{i,k} = i_{\mathrm{meas},k} - i_{\mathrm{meas},k-1}$ are parametrized using the measured step responses. The sampling time is T_S and $t = k \cdot T_S$. The output i_{mod} is the model equivalent to i_{meas}, while $i(f,q)$ results from the nonlinear-static part of the model (3) - (5). The dynamic model part (6) therefore requires to have unity gain. The model order n depends on the sampling time and the time constants of the system, as the model has to cover the whole transient step response. We will use a lower sampling time $T_S = 1$s for the UKF which results in $n = 3$, while the decision algorithm requires a finer time resolution with $T_S = 0.01$s and $n = 150$.

Fig. 2 depicts the model structure, where from left to right the normalized flow rate q_{norm} results from (3) and the inputs f and q, then i_{norm} follows from (5), f and q_{norm}. The normalized current i_{norm} is then de-normalized with (4) and f. The resulting i is the input for the linear dynamic part of the model (6), which then yields $i_{\mathrm{mod}}(q, f, t)$ as output.

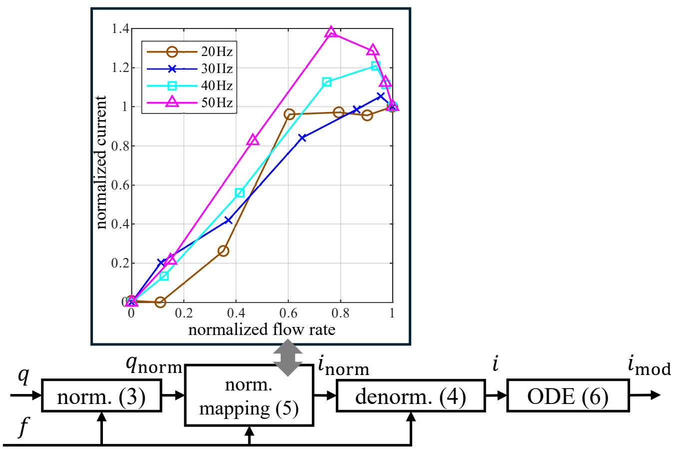

Fig. 2. The enhanced BCM model maps the flow rate and frequency to electrical current through a series of non-linear static functions and incorporates the transient behaviour with a linear-dynamic model part.

3.2 Unscented Kalman Filter

We implement the Unscented Kalman Filter following Julier and Uhlmann (1997). The nonlinear-dynamic model (6) serves as the state update function. We define the state vector $x_i(k)$ from (6) as state variables $x_1(k)$ to $x_n(k)$ within the UKF. Since the static model $i(f,q)$ is part of (6) and requires q as input, which is unknown as it is the desired estimate, we define q as additional state variable $x_{n+1}(k)$ with $x_{n+1}(k+1) = x_{n+1}(k)$, thus treat it as an estimated parameter. The frequency f serves as the input u, while the measured electric current i_{meas} is treated as the system output y. Consequently, the state update model can be formulated as

$$
\begin{pmatrix} x_1(k+1) \\ \vdots \\ x_n(k+1) \end{pmatrix} = A \cdot \begin{pmatrix} x_1(k) \\ \vdots \\ x_n(k) \end{pmatrix} + b \cdot i(u(k), x_{n+1}(k))
$$

$$
x_{n+1}(k+1) = x_{n+1}(k)
$$

$$
y(k) = c \cdot \begin{pmatrix} x_1(k) \\ \vdots \\ x_n(k) \end{pmatrix} . \tag{7}
$$

We then have the estimates $\hat{i}(k) := y(k)$ and $\hat{q}(k) := x_{n+1}(k)$ as result from the UKF algorithm.

In this standard formulation, the UKF is unable to decide between two estimates $\hat{q}^+$ and $\hat{q}^-$ whenever both yield the same estimated $\hat{i}$, likely resulting in a wrong $\hat{q}$. The decision algorithm presented in the following Sects. 3.3 and 3.4 implements the selection of the correct $\hat{q}$.

3.3 Decision criterion

We denote the lowest current for which a second flow rate estimate exists by i_{lim}. In Fig. 1, i_{lim} would be at around 60% for the simple non-invertible case. As long as $i_{\mathrm{meas}} < i_{\mathrm{lim}}$, no further decision is required as the estimate $\hat{q}$ is unique.

The decision algorithm is based on a frequency step $f = \overline{f} - \Delta f$ and step response analysis. According to the hydraulic affinity laws, a reduced frequency leads to a reduced electrical current $i \propto f$ and a reduced flow rate $q \propto f$, assuming that the process parameters remain constant (e.g. no valve position is changed). The transient response in i to the frequency step can be split into the immediate effect associated with the reduced f and a subsequent change due to the following reduction in q, due to fluid inertia. Fig. 3 illustrates the transient response of the operating point. There, $i_0 = i(\overline{f}, q_0)$ is the initial steady-state, and $i_1 = i(f, q_0)$ results from reducing the frequency to $f = \overline{f} - \Delta f$ while the flow rate approximately remains constant at its initial value q_0. Consequently, $i_1 - i_0$ is the initial reduction in i due to the frequency step. The subsequent change due to the reducing flow rate $q_0 \to q_2$ yields $i_2 = i(f, q_2)$. If q_0 and q_2 are located left of the maximum in the $q \to i$ curve, the reduced flow rate leads to a further decrease in i. Conversely, if q_0 and q_2 are both located right of the maximum in the $q \to i$ curve, the reduced flow rate leads to an increase on i:

$$
i_2 - i_1 \begin{cases} < 0 & : \ q_0 \text{ and } q_2 \text{ left of maximum} , \\ > 0 & : \ q_0 \text{ and } q_2 \text{ right of maximum} . \end{cases} \tag{8}
$$

In Fig. 3, left of the maximum, i first decreases from i_0^- to i_1^-, due to the frequency step, and then further decreases from i_1^- to i_2^-. On the right side of the maximum, the current first decreases from i_0^+ to i_1^+ and subsequently rises again from i_1^+ to i_2^+. Points i_1^{++} and i_2^{++} result from a frequency step with larger Δf (see Sec. 3.4).

We stress here that the steady-state values i_2^+ and i_2^- are equal for equal starting points $i_0^+ = i_0^-$, which follows from the hydraulic affinity laws. Consequently, the transient response needs to be evaluated, since the steady state does not contain the relevant information.

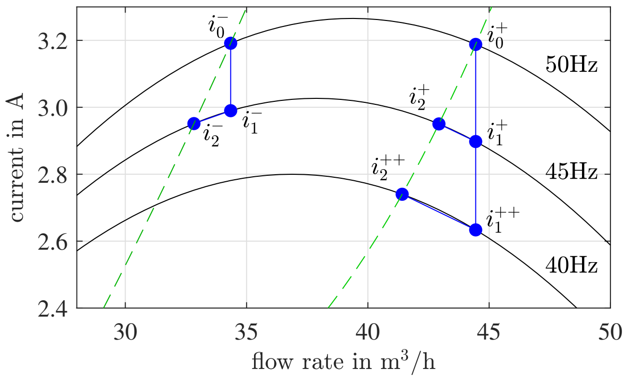

Fig. 3. Illustrated effect of a frequency step from 50Hz to 45Hz and to 40Hz. The black curves are the corresponding $q \to i$ curves and the green dashed curves depict two example plant characteristics. The blue lines visualize the electrical power responses combined of the immediate frequency step effect and the subsequent effect of the reducing flow rate. Superscripts $-$ and $+$ indicate the "left-of-maximum" and "right-of-maximum" cases, respectively, as in (8). Superscript $++$ indicates operating points resulting from a frequency step with larger Δf.

The measurable response in $i(t)$ is a combination of the response related to the operating point transition $i_0 \to i_1^{\pm} \to i_2^{\pm}$, which we will denote by $i_{\text{op}}(t)$, and a response related to pump and motor inertia and possible lag effects in the sensing equipment, $i_{\text{S}}(t)$. Their superposition yields the measurable response $i(t) = i_{\text{op}}(t) + i_{\text{S}}(t)$. The transient response $i_{\text{S}}(t)$ is independent of the operating point, while $i_{\text{op}}(t)$ changes with the location left or right of the maximum in the $q \to i$ curve. Consequently, a distinguishable transient response in $i(t)$ will result. Measuring the actual response in $i(t)$ and separating $i_{\text{S}}(t)$ yields a decision criterion. In discrete time, this criterion reads

$$\sum_{k=0}^{n} i(k) - i_S(k) \begin{cases} > 0: & \hat{q}^* = \hat{q}^+ \\ < 0: & \hat{q}^* = \hat{q}^- \end{cases}, \tag{9}$$

where the time span $0 \leq kT_S \leq nT_S$ covers the full transient response of $i(t)$.

3.4 Towards a decision algorithm

The response i_S corresponds to the model (6), as the model was identified with excluded flow rate effects ($q = 0$). We therefore have $i_S(t) = i_{\text{mod}}(t)$ for a step in f and fixed q, and can compare this response with a measured step response $i_{\text{meas}}(t)$ to obtain information about i_{op}. The left diagram in Fig. 4 depicts two step responses $i - i_{\text{S}}$ over q for part-load and overload operation. The trajectories coincide well with the previous discussions (cf. Fig. 3). The right diagram in Fig. 4 depicts the two step responses $i(t)$ over time together with a response without the operating point transition, $i_{\text{S}}(t)$. Criterion (9) is obviously fulfilled in both cases.

The measurable difference between i and i_{S} depends on the flow rate and usually decreases with lower flow rates,

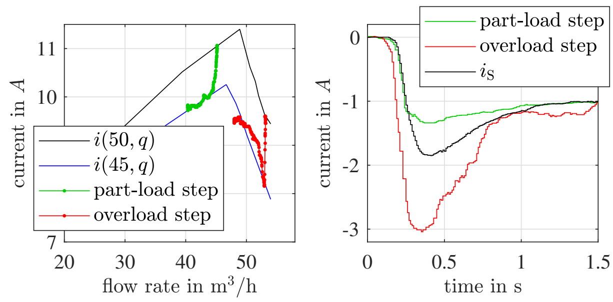

Fig. 4. Left: Two step responses $i - i_{\text{S}}$ over q, for part-load and overload operation. Right: Two step responses $i(t)$ for part-load and overload operation for a step in f and the model response $i_{\text{S}}(t) = i_{\text{mod}}(t)$ for a step in f and fixed q.

which, combined with measurement noise, may render (9) below a minimum flow rate. An increased frequency step with larger Δf is then required, as evident from Fig. 3 for $i_0^+ \to i_1^{++} \to i_2^{++}$, as the flow rate related effects increase with the step amplitude.

If the noise bound for i_{meas} is known, i.e. $\alpha < i_{\text{meas}}(k) < \beta$ for all k, a criterion for a sufficient Δf can be formulated using an inequality (Hoeffding, 1994)

$$\Pr\left[i_{\text{meas}}(k) - \mathrm{E}\left[i_{\text{meas}}(k)\right] \geq \kappa\right] \leq \exp\left(\frac{-2n\kappa^2}{(\beta-\alpha)^2}\right), \tag{10}$$

where $\mathrm{E}\left[i_{\text{meas}}(k)\right] = i(t)$, i.e. the expected transient response without disturbance, and n is the sample count, i.e. the order n of the dynamic model (6), and depends on T_S and the measured timespan of the step response, which has to cover the response until it is sufficiently close to the new steady-state. Then (10) yields the probability for a deviation of the measured response $i_{\text{meas}}(k)$ from the expected response $i(k)$ by a factor larger than κ. If we choose

$$\kappa = \min\left(|i_1^+ - i_2^+|, |i_1^- - i_2^-|\right) \tag{11}$$

for the case in which the response i_{meas} deviates from the expected response $i(t)$ by a value larger than the difference between $i_1^{\pm}$ and $i_2^{\pm}$, i.e. the basis of the decision criteria (8) and (9). The difference in (11) result from the steady-state model $i(f, q)$. With the two possible estimates $\hat{q}^+$ and $\hat{q}^-$ we get $i_1^{\pm} = i(f, q_1^{\pm})$ and $i_2^{\pm} = i(f, q_2^{\pm})$, where $q_1^{\pm} = \hat{q}^{\pm}$ prior to the frequency step (see Fig. 3), and $q_2^{\pm} = \hat{q}^{\pm} \cdot f/\overline{f}$, i.e. the final steady-state flow rate at the end of the transient response, according to the hydraulic affinity law $q \propto f$. Since the difference between q_1 and q_2 depends on the difference $\overline{f} - f = \Delta f$, κ is proportional to Δf. We thus have a way to decrease the probability of measurement deviation in (10) by increasing Δf, while n, α, and β result from the system properties (duration of the transient response and the noise in i_{meas}, respectively).

We show a sample application with a fixed Δf in the following section but note here that Δf could be adjusted iteratively (i.e. increased when the probability from (10) exceeds a desired threshold). The algorithm and the application of the frequency steps may require additional, problem specific adaptations, e.g. when the pump is embedded into a closed loop control or is required to guarantee a certain flow rate (cf. Leonow and Mönnigmann (2016)).

4. PRACTICAL APPLICATION

We implemented the combination of UKF and decision algorithm in a laboratory setup. The setup involves a standard centrifugal pump with simple non-invertible characteristic (cf. Fig. 2 for the characteristics at four different frequencies, measured at the test pump) and variable frequency drive (VFD). We included a downstream valve to simulate variable hydraulic parameters and to deliberately move the operating point across the maximum of the $q \to i$ curve. The pipe system length is 10m, which induces a relatively low fluid inertia. The measurement of i_{meas} is performed by the VFD. A flow meter yields the true q_{meas} and is included to evaluate the soft sensor performance. Data acquisition and implementation of the algorithms is achieved by a Matlab and Simulink connection to the plant via an i/o-card. The measured i_{meas} contains a substantial amount of noise due to electromagnetic disturbances from the VFD.

The setup allows for a frequency range of 20 Hz to 50 Hz, associated with a rotational speed range of 1200 rpm to 3000 rpm. The flow rate can achieve a maximum of about 60 m^3/h with 50 Hz and full open valve.

4.1 Soft sensor implementation

We use (7) as state update model with $n = 3$ for the UKF. The tuning parameters of the UKF were chosen as

$$Q = \text{diag}\,(0.001 \cdot c \ , \ 10) \ \ , \quad r = 0.01$$

and the sample time is $T_S = 1$s.

For the decision algorithm, (6) is used with $n = 150$ and a sample time $T_S = 0.01$s, thus covering 1.5s of transient response. For simplicity, we apply a frequency step with a fixed $\Delta f = 5$Hz every 20s. The decision algorithm has full authority over f.

We implement the UKF twice and limit the parameter ranges for x_{n+1} to the range left of the maximum and right of the $q \to i$ curve maximum, so that the UKF yield $\hat{q}^+$ and $\hat{q}^-$, respectively. The decision algorithm then selects $\hat{q}^* = \hat{q}^+$ or $\hat{q}^* = \hat{q}^-$, according to the result of (9). The setup is depicted in Fig. 5.

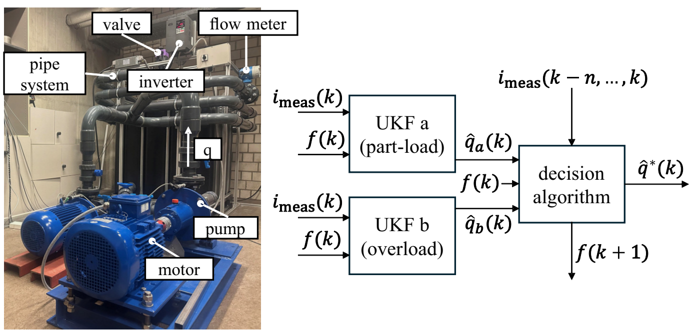

Fig. 5. Left: photograph of the test stand. Right: setup of the soft sensor with dual UKF and decision algorithm.

4.2 Experimental Result and Discussion

We conducted a 10 minute test run of the soft sensor and changed the operating point from part-load to overload operation and back. The upper diagram in Fig. 6 depicts the measured i_{meas} and the two estimates $\hat{i}^{\pm}$ from UKF+ and UKF-. The substantial noise amount in i_{meas} is evident.

The middle diagram in Fig. 6 holds the estimated flow rates $\hat{q}_{a,b}$, the measured flow rate q_{meas}, and the decision $\hat{q}^*$. The gray, red and green colored bar at the bottom of the diagram shows the decision. It is evident that the decision $\hat{q}^*$ reflects the true flow rate q_{meas} well. At $t = 500$s, where the flow rate transitions back to the part-load side, the decision algorithm requires two speed steps for a reliable decision. Therefore, the estimate $\hat{q}^*$ follows $\hat{q}^+$ for about 40s, while $\hat{q}^-$ would be correct, exposing the limitation of the algorithm due to the close proximity of $\hat{q}^+$ and $\hat{q}^-$ in combination with the substantial noise in i_{meas}. Note that a wrong decision is likely to occur when $\hat{q}^+$ and $\hat{q}^-$ are close, however, the resulting estimation error is consequently also small.

The lower diagram in Fig. 6 depicts the frequency f, which performs a step with $\Delta = 5$Hz every 20s.

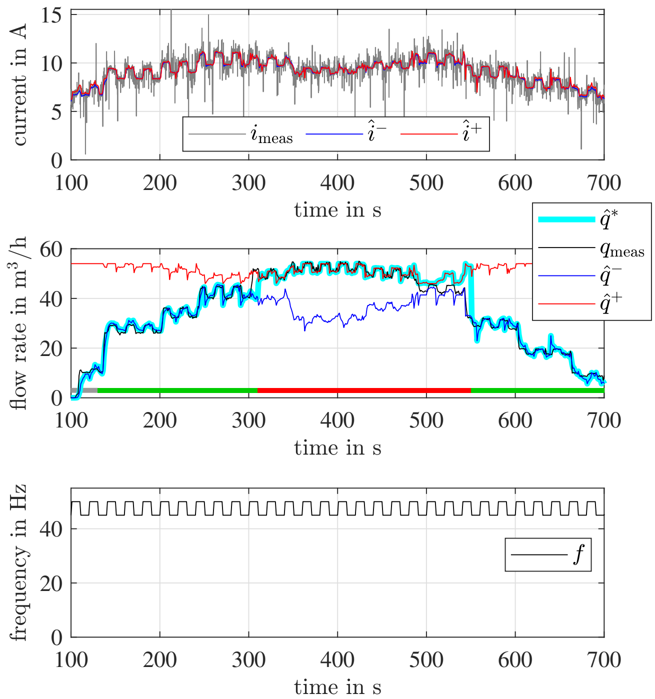

Fig. 6. Time series of a 10 minute evaluation of the soft sensor. The upper diagram compares measured and estimated currents i, the middle diagram compares measured and estimated flow rates q. The lower diagram depicts the frequency f.

Fig. 7 summarizes the steady-state precision of the soft sensor by comparing the measured steady-state operating points $(q_{\text{meas}}, i_{\text{meas}})$ with the estimated counterparts $(\hat{q}^*, \hat{i}^*)$. The blue line depicts the $q \to i$ curve from the static model $i(f, q)$. Overall, a high coincidence between model, measured, and estimated data is given. The standard deviations σ for $\hat{q}^*$ and the measured i_{meas} indicate that the noise in i_{meas} is amplified in $\hat{q}^*$, due to the flat

$q \to i$ curve. The lower diagram in Fig. 7 depicts the decision within criterion (9), i.e. $\sum_{k=0}^{n} i(k) - i_f(k)$, and the probability of significant deviations in the measured step response $\Pr[i_{\text{meas}}(k) - \mathrm{E}[i_{\text{meas}}(k)] \geq \kappa]$ from (10), labeled uncertainty in Fig. 7, over q. From i_{meas} we identified $\alpha = 2.7$ and $\beta = 8.1$ for a steady-state situation.

For low part-load operating points, the uncertainty of the estimation becomes large as expected due to the reduced effect of the frequency step onto q and the flat $q \to i$ curve. As the operating points shifts towards larger q, the uncertainty decreases in the predicted fashion. At $q \approx 30\text{m}^3/\text{h}$, the operating points enters the ambiguous region with i_{meas} exceeding i_{lim} and the decision is reliable throughout the whole ambiguous region. At $q \approx 45$, the decision changes from part-load to overload, corresponding to the operating point traversing the maximum in the $q \to i$ curve.

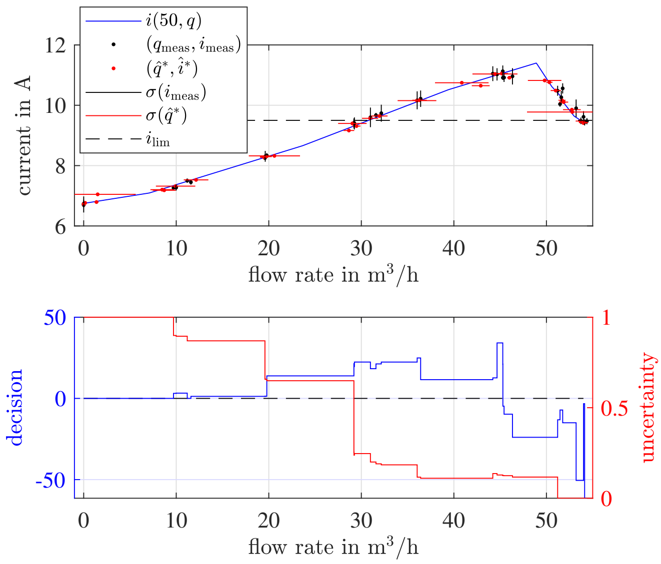

Fig. 7. Upper diagram: comparison of measured and estimated flow rates q and currents i with standard deviations σ for measured current and estimated flow rate. Lower diagram: decision and uncertainty values from (9) and (10), plotted over the flow rate.

5. CONCLUSION

The proposed flow rate soft sensor demonstrates significant potential for improving real-time flow monitoring in centrifugal pumps, addressing the challenge of non-invertible characteristics under noisy measurement conditions. The decision algorithm evaluates the transient response of the measured current and concludes if the operating point is left or right of the maximum in the $q \to i$ curve.

We note that, in contrast to out previous publication Leonow and Mönnigmann (2016), the algorithm proposed here is more practical and showed promising results in the real application. Also, the pipe system length was 10m here, where we required 200m in our previous work for a sufficient inertia and pronounced transient response of the flow rate q. We further note that the proposed algorithm does not require extensive data from the pump system, which deliberately sets it apart from any machine learning approach.

In future works, we will implement the decision algorithm in a more adaptable format, by identifying Δf automatically and by preventing step response measurement in transient situations, e.g. during adjustments by an external controller when integrated into a closed-loop control.

ACKNOWLEDGEMENTS

This work is funded by Germany federal ministry for economic affairs and climate action.

REFERENCES

Ahonen, T., Tamminen, J., Ahola, J., Viholainen, J., Aranto, N., and Kestilä, J. (2010). Estimation of pump operational state with model-based methods. *Energy Conversion and Management*, 51(6), 1319–1325.

Becker, T. and Krause, D. (2010). Softsensorsysteme. Mathematik als Bindeglied zum Prozessgeschehen (in german). *Chemie Ingenieur Technik*, 82(4), 429–440.

Changklom, J. and Stoianov, I. (2019). Redundant flow estimation methods for robust hydraulic control in water supply networks. *Journal of Hydroinformatics*, 21(4), 571–592.

Chhantyal, K., Viumdal, H., and Mylvaganam, S. (2017). Soft sensing of non-newtonian fluid flow in open venturi channel using an array of ultrasonic level sensors—ai models and their validations. *Sensors*, 17(11), 2458.

Hoeffding, W. (1994). *Probability Inequalities for sums of Bounded Random Variables*, 409–426. Springer New York, New York, NY.

Julier, S.J. and Uhlmann, J.K. (1997). New extension of the kalman filter to nonlinear systems. In *Signal processing, sensor fusion, and target recognition VI*, volume 3068, 182–193. Spie.

KSB-AG (2005). Flow rate measurement (in german). *German Patent DE10359726A1*.

Leonow, S. and Mönnigmann, M. (2013). Soft sensor based dynamic flow rate estimation in low speed radial pumps. In *2013 European Control Conference (ECC)*, 778–783. IEEE.

Leonow, S. and Mönnigmann, M. (2016). Operating point estimation in hydraulic turbomachines with non-invertible characteristics. In *2016 European Control Conference (ECC)*, 2380–2385. IEEE.

Leonow, S., Zhang, Q., and Mönnigmann, M. (2024). A modular soft sensor for centrifugal pumps. *IFAC-PapersOnLine*, 58(14), 91–96.

Lima, R.P.G., Mauricio Villanueva, J.M., Gomes, H.P., and Flores, T.K.S. (2022). Development of a soft sensor for flow estimation in water supply systems using artificial neural networks. *Sensors*, 22(8), 3084.

Lin, Y., Li, X., Zhu, Z., Wang, X., Lin, T., and Cao, H. (2022). An energy consumption improvement method for centrifugal pump based on bionic optimization of blade trailing edge. *Energy*, 246, 123323.

Ren, L., Wang, T., Laili, Y., and Zhang, L. (2021). A data-driven self-supervised lstm-deepfm model for industrial soft sensor. *IEEE Transactions on Industrial Informatics*, 18(9), 5859–5869.

Sedghi, S., Tan, R., and Huang, B. (2020). Data analytics approach for online produced fluid flow rate estimation in sagd process. *Computers & Chemical Engineering*, 136, 106766.

Shankar, V.K.A., Umashankar, S., Paramasivam, S., and Hanigovszki, N. (2016). A comprehensive review on energy efficiency enhancement initiatives in centrifugal pumping system. *Applied Energy*, 181, 495–513.

Wu, Y., Wu, D., Fei, M., Sørensen, H., Ren, Y., and Mou, J. (2023). Application of ga-bpnn on estimating the flow rate of a centrifugal pump. *Engineering Applications of Artificial Intelligence*, 119, 105738.